A Robust Anticorrosive Coating Derived from Superhydrophobic, Superoleophobic, and Antibacterial SiO_2@POS/N^+ Composite Materials

Congcong Miao,[1] Congcong Li,[2] Xiaoxue Huang,[2] Tiantian Yang,[2] Yue Wang,[1] Junqiu Mao,[1] Yanfang Wang,[1] Xiang Cui,[1*] Haidong Xu[1*] and Xiaofeng Wu[3*]

[1]Normal College for Nationalities, College of Chemistry and Chemical Engineering, Qinghai Normal University, Xining, 810008, PR China

[2]College of Petrochemical Engineering, Lanzhou University of Technology, Lanzhou 730050, PR China

[3]Department of Chemistry, University of Liverpool, Liverpool, UK L69 7ZD

Corresponding E-mails: 373498635@qq.com; lzxhd123@sina.com; xfwu@liverpool.ac.uk

Abstract

Traditional coatings are easily susceptible by the contamination of organic pollutants and parasitism of bacterium, resulting in severe corrosion damage to the protected substrates. The coating with superhydrophobic, superoleophobic and antibacterial properties would not only spontaneously form an air layer when it is immersed into corrosive medium and effectively obstruct corrosive medium to devastate metal matrix, but also be beneficial to improve the coating's anti-fouling performance along with its antibacterial functionality. However, traditional anticorrosive methods are problematic with low anticorrosion efficiency and single function. Herein, a robust anticorrosive coating stemmed from superhydrophobic, superoleophobic, and antibacterial SiO_2@POS/N^+5 composite was prepared by sol-gel and spray method, with water contact angle and water sliding angle up to 160.8 ± 3.1° and 3.0° and oil contact angle and oil sliding angle up to 152.5 ± 3.0 and 3.0° were achieved, respectively. The SiO_2@POS/N^+5 coating has excellent protection performance (99.98%), mechanical properties and corrosion durability (21 d). Notably, the SiO_2@POS/N^+5 composite material has excellent antibacterial effect against *Staphylococcus aureus* (*S. aureus*) (100%) as well. The superamphiphobic coating proposed in this study affords a feasible strategy for bacterial contamination of metal surfaces in marine industries.

Keywords: Superhydrophobicity, Superoleophobicity, Anticorrosive, Antibacterial

1. Introduction

Artificial bionic superhydrophobic surface, inspired by a large number of natural phenomena such as the self-cleaning lotus leaves, the "water-resistant" legs of water striders, the water-repellent wings of butterflies and the antifogging property of mosquito eye, has found enormous applications in both industry and domestic daily life.[1,2] Meanwhile, the problem of water pollution all over the world has been aggravated in recent years, dominating by organic pollutants in water resources such as oil leakage, industrial sewage discharge, direct discharge of domestic sewage, etc., which raises the increasing demand of coatings applied in severe sewage environments.[3,4] The coatings with superoleophobic functionality would be ideal for resolving these problems. Furthermore, the superhydrophobic surface along with superoleophobic functionality simultaneously (also known as superamphiphobic) has a wide range of applications in self-cleaning, anti-icing, anticorrosion, and antibacterial aspects and countless

requirements for the surface maintenance and protection such as mobile, car, piano, and luxury furniture etc., possessing with high contact angle (> 150°) and low sliding angle (< 10°).[5-11]

On the other hand, corrosion causes significantly economic losses and life-threaten to health and environment globally.[12,13] Alleviating metal corrosion is essential and even crucial to marine and many other industries as well as the academic researches, including protective coatings,[14-16] cathodic protection,[17] or corrosion inhibitors,[18] etc. However, traditional anticorrosive methods are problematic with their low anticorrosion efficiency and single function, which circumvents the practical necessity. In the actual complex marine environment, the surface of metal equipment will not only be damaged by corrosive media such as H_2O and Cl^-,[19] but also be parasitized by a large number of microorganisms, causing the degradation of organic coatings.[20] For example, after the bacteria attach to the surface of marine equipment, they will colonize the surface to form biofilms according to the adaptive mechanism. The bacteria will then be embedded in the biofilm, which is extremely difficult to remove subsequently, seriously limiting the service lifetime and devastating the functionality of metals.[21-26] Therefore, practical applications require the development of anticorrosive coatings with antibacterial property to resist the attachment and parasitism of microorganism.

The antibacterial superamphiphobic coating shows important and valuable applications in the anticorrosion of ocean shipping equipment, significantly reducing the erosion of the surface performance of hulls or marine equipment by those microorganisms as well as avoiding the formation of biofilms on hull and pipeline coatings as its antibacterial properties.[27-29] An air layer would spontaneously form on the surface when the superamphiphobic surface is immersed into corrosive medium, which can effectively obstruct corrosive medium to demolish metal matrix.[30,31] The antibacterial mechanism of superamphiphobic surface is considered as anti-adhesion surface, which results in the rolling of water droplets to remove bacteria away, giving little chance for bacteria to adhere to the surface.[32, 33] In 2022, Wang *et al.* [34] reported a sprayable coating with superhydrophobic and antibacterial performances, which reduced adhesion to *Escherichia coli* (*E. coli)* and *Staphylococcus epidermidis*. However, the anti-adhesion of superhydrophobic surfaces does not completely eliminate bacteria. Compared with monofunctional antibacterial coatings, bifunctional antibacterial coatings with both anti-adhesion and bactericidal properties showed preeminent performance in antibacterial adhesion and prevention of biofilm formation.[35] Therefore, in the construction of the microstructure of superamphiphobic composites, it is of great significance to ingeniously introduce antibacterial agents to prepare superamphiphobic surfaces that are both resistant to bacterial adhesion and sterilization. The exploration of antibacterial agents has broad application prospects in the development of sterilization surfaces, such as natural antibacterial substances (e.g., chitosan),[36] inorganic antibacterial agents (e.g., copper, silver, TiO_2, ZnO) [37-40] and organic antibacterial agents (e.g., quaternary ammonium salts (QASs)).[41, 42] Among them, QASs have the outstanding cell membrane permeability, good environmental stability, inferior toxicity, fewer skin irritation and reinforced biological activity.[43] Yang *et al.* [44] modified gelatin (GE) with epoxysiloxane quaternary ammonium salt (EPSiQA) under alkaline conditions (pH 10-11), so that silyl groups and quaternary ammonium groups were simultaneously grafted to the gelatin backbone. The results showed that EPSiQA-GE had good bactericidal effect to the Gram-positive bacteria.

In this paper, a superamphiphobic and antibacterial composite material was prepared by hydrolyzed polycondensation reaction with significantly improved anticorrosion functionality. Thus, the SiO_2 nano-particles (SiO_2) embedded into the hydrolyzed polycondensation products (POS) of (3-mercaptopropyl)trimethoxysilane (MPS) and trimethoxy(1H,1H,2H,2H-heptadecafluorodecyl)silane (TMFS) to construct micro/nano roughness, in which the POS and hexadecyl trimethyl ammonium

bromide (CTAB) would reduce the interface energy of the composite materials. Of particular note is that the CTAB, a type of quaternary ammonium salt, has excellent antibacterial property due to its cell-walls-destroyable function by N^+ ions, affording both anti-adhesion surface and antibacterial surface for the obtained composite coating. The resultant functional material (SiO_2@POS/N^+) was sprayed on the substrate, with the assistant of the 3M 75 adhesive spraying to improve the mechanical properties of the coating.

2. Experimental

2.1 The preparation of SiO_2@POS/N^+

A certain amount of SiO_2 and 45 mL absolute ethanol was added into a 100 mL round-bottomed flask and stirred for 30 min to disperse adequately, then 0.4 mM CTAB (14.6 mg), 15 mM TMFS (434.9 mg) and some of MPS were added into the dispersion and stirred until dissolved completely. With the addition of distilled water (5 mL), the mixture was stirred vigorously at 60 °C for a certain time. After cooling down to the room temperature, a white suspension was obtained (termed as SiO_2@POS/N^+), the SiO_2@POS/N^+ of different additive amount is labeled SiO_2@POS/N^+1-10 in Table 1, respectively, and used directly for the next step without any further purification.

2.2 The preparation of SiO_2@POS/N^+ coating

After a portion of the obtained SiO_2@POS/N^+ dispersion (5 mL) was added into the airbrush (CM-CP2, 0.23 mm) connected to the U-601G type air pump, the targeted glass slide surface (25 mm × 25 mm) was sprayed with 3M75 glue in prior and then evenly sprayed with these dispersed nanoparticles solution by the air pump (25 PSI). The resultant specimens were placed at room temperature for 30 min, then dried at 60 ℃ for 12 h, and measured the water contact angle (WCA), water gliding angle (WSA), oil contact angle (OCA) and oil contact angle (OSA) of the resultant coatings subsequently (labeled as SiO_2@POS/N^+1-10 coating).

2.3 Anticorrosion experiment

Q235SS alloy (25 mm × 10 mm × 0.5 mm), polished with 800 grit sandpaper to remove the passivation layer on the surface, was ultrasonically cleaned in ethanol and distilled water for 10 minutes, respectively, and then dried naturally in the air. The electrode of Q235SS was wrapped with tape except the targeted exposed test area (1 cm^2) around the bottom dipped in the electrolyte as well as the top connection point. For the corrosion durability test samples, the metal matrix was protected with a complete and perfect seal by the glue-302 modified acrylate adhesives surrounding the coating area and was then cured at room temperature for 12 h prior to the corrosion durability test. The designed coating was prepared by the spraying the dispersed solution of SiO_2@POS/N^+ onto the Q235SS alloy and dry it in an oven at 60 °C for 12 h. A three-electrode electrochemical workstation system was adopted, with the counter electrode of a platinum wire, the reference electrode of saturated calomel electrode (SCE), the working electrode of bare Q235SS alloy or SiO_2@POS/N^+ coated Q235SS alloy, and the electrolyte of composed of 3.5% NaCl aqueous solution. The Tafel curve at a rate of 10 mV/s of the exposed coating surface was then measured within -1.0～1 V range to clarify the anticorrosion effect.

2.4 Impedance experiment

The SiO_2@POS/N^+ coated Q235SS alloy was prepared according to the method described in section 2.3, and the same test method to that in 2.3 applied as well. The coating was inserted into the 3.5% NaCl solution, standing for 30 min. The open-circuit potential (E_{ocp}) was obtained by remaining unchanged within 3 min after the decimal point to three digits, and the EIS frequency range 10^{-2}～10^5 Hz, and amplitude is 0.005 V.

2.5 Antibacterial experiment

Antibacterial activity of the SiO_2@POS/N^+ composite material was evaluated by the plate count method. Gram-positive *S. aureus* and Gram-negative *E. coli* were selected as representative bacterial strains. Single colonies of *E. coli* and *S. aureus* strain were selected from the Luria-Bertani (LB) agar plate and inoculated in LB fluid nutrient medium (50 mL). Bacteria suspensions were grown under shaking (200 rpm) at 37 ℃ for 18 h. The suspensions were diluted by phosphate buffered saline (PBS) solution to acquire 10^6 CFU/mL bacteria samples. To evaluate the antibacterial properties of SiO_2@POS/N^+5 (200 mg) was co-cultivated with bacteria, and the blank group, only the bacteria solution was added without the sample, and it was placed in a constant temperature shaking (200 rpm) at 37 ℃ for 6 h. After the culture completion, PBS solution was conducted to dilute the culture solution continuously by 10 times (three dilution multiples of 10^5, 10^6 and 10^7), and then the resultant diluted solution (120 μL) was taken and spread evenly on the LB solid medium. The resultant plate was then placed in a constant temperature incubator at 37 ℃ for 18 h, observing and taking pictures to record the number of colonies. Each group was set up with 2 parallel repetitions. In addition, all samples and utensils in the experiment were sterilized in prior in a high-temperature and high-pressure steam sterilizer at 121 ℃ for 30 min. Chemicals and materials, characterization methods and other experimental sections please refer to the supplementary information (SI) for more details.

The schematic diagram of the preparation SiO_2@POS/N^+ coating is shown in Fig. 1. Thus, Fig. 1a represents Q235SS. Fig. 1b represents SiO_2@POS/N^+ coating, in which the blue balls represent adhesive layer with the function of effective improvement of the mechanical properties of coating, the red balls represent superamphiphobic layer which is consisted of SiO_2, CTAB and POS; the SiO_2 is used to construct enough micro/nano roughness, and the POS and CTAB can reduce the interface energy to achieve superamphiphobicity, while CTAB has excellent antibacterial properties with its quaternary ammonium salt functional group. Thus, an air layer would spontaneously generate and obstruct the immersion of corrosive mediums, the translucent blue balls and translucent yellow balls represent water drops and hexadecane oil drops, respectively. They couldn't immerse into the SiO_2@POS/N^+ coating in Fig. 1b. Fig. 1c is representative reaction scheme for hydrolytic polycondensation of SiO_2@POS/N^+, in which the -OH, -SH in POS and N^+ functional groups in CTAB have weak interaction with -OH on SiO_2 surface and would facilitate the formation of the micro structure of SiO_2@POS/N^+ particles.

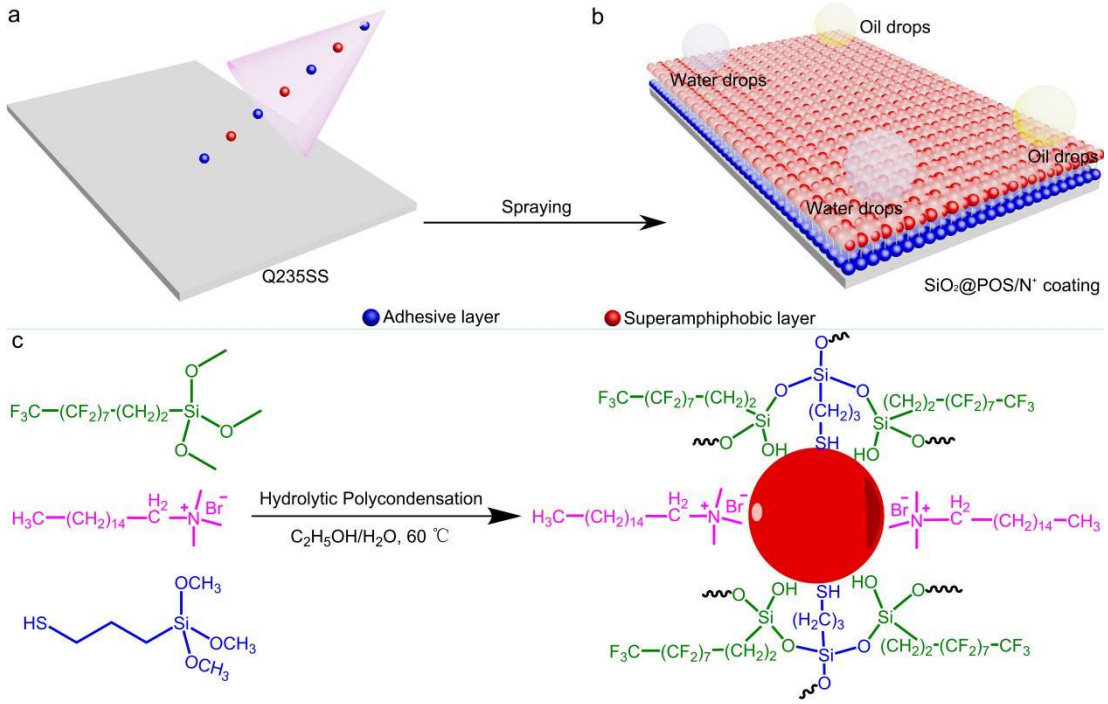

Figure 1. The schematic diagram of the preparation of SiO_2@POS/N^+ coating. Q235SS (a); SiO_2@POS/N^+ coating (b), in which the translucent blue balls represent water drops, the translucent yellow balls represent hexadecane oil drops; the reaction scheme of hydrolytic polycondensation (c).

3. Results and Discussion

3.1 Synthesis and Characterizations of SiO_2@POS and SiO_2@POS/N^+5

With the materials synthesized according to the methods and procedures aforementioned, the FTIR has been firstly conducted to characterize the composition of composite materials. Fig. 2a and 2b are FTIR spectra of SiO_2@POS and SiO_2@POS/N^+5, the SiO_2@POS represents the sample without CTAB when the SiO_2@POS/N^+5 is prepared under the same conditions. The absorption band of 3402 cm^{-1} is assigned to the vibration peak of Si-OH and H_2O in Fig. 2a and 2b,[45, 46] the anti-symmetric and symmetrical stretching vibration peaks of methylene are around 2917 cm^{-1} and 2851 cm^{-1},[45] the peaks at 2967 cm^{-1} and 2917 cm^{-1} are attributed to the symmetrical and asymmetrical stretching vibration of the C-H of -CH_2 in TMFS,[47] the peak at 1232 cm^{-1} belongs to the stretching vibration of C-F in POS,[48] the peak at 1067 cm^{-1} is attributed to the stretching vibration of Si-O-Si in POS and SiO_2,[49, 50] the peak at 808 cm^{-1} is attributed to the bending vibration of Si-O bond.[51]

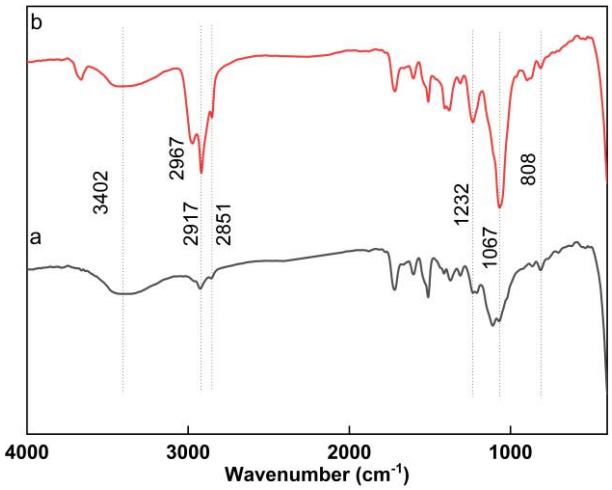

Figure 2. The FTIR spectra of SiO_2@POS (a) and SiO_2@POS/N^+5 (b)

In addition, the composition of SiO_2@POS/N^+5 is analyzed by energy dispersive spectroscopy (EDS) as shown in Fig. 3. The SiO_2@POS/N^+5 composite material and its corresponding EDS spectrum are shown in Figs. 3a, 3b, respectively. In Fig. 3b, the elements of O and Si are mainly derived from POS and SiO_2, the molar ratio of O and Si is about 2:1. The existence of the elements of N and Br indicates that the CTAB has been successfully introduced into SiO_2@POS/N^+5, so were the existence of S element as to the MPS. The F element in the composite is mainly derived from TMFS in POS. The FTIR and EDS spectra revealed that the SiO_2@POS/N^+5 composite is successfully prepared.

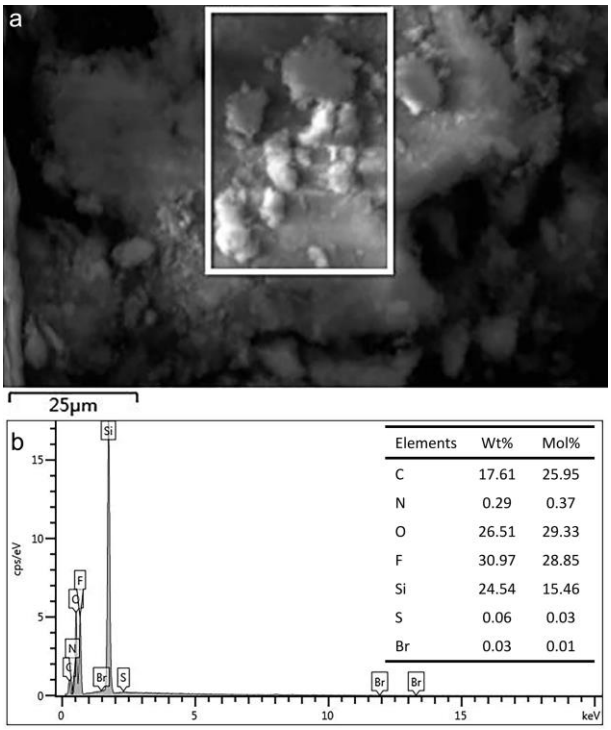

Figure 3. The SEM image of EDS corresponding samples (a), the EDS image of SiO_2@POS/N^+5 (b).

The superamphiphobic of SiO_2@POS/N^+ coatings are particularly related to micro/nano roughness, which can be analyzed by SEM image. Figs. 4a, 4b, 4c and 4d are X5000, X10000, X20000 and X3000 SEM images of SiO_2@POS/N^+5 coating. The coating surface has good uniformity as shown in Fig. 4a, whilst it has enough micro/nano roughness as indicated in Figs. 4b and 4c and the great mass of particles size of SiO_2@POS/N^+ coating is about 80 nm ~ 100 nm (Fig. 4d). It is evidenced that SiO_2@POS/N^+5

coating have good micro/nano roughness to construct the superamphiphobic surface.

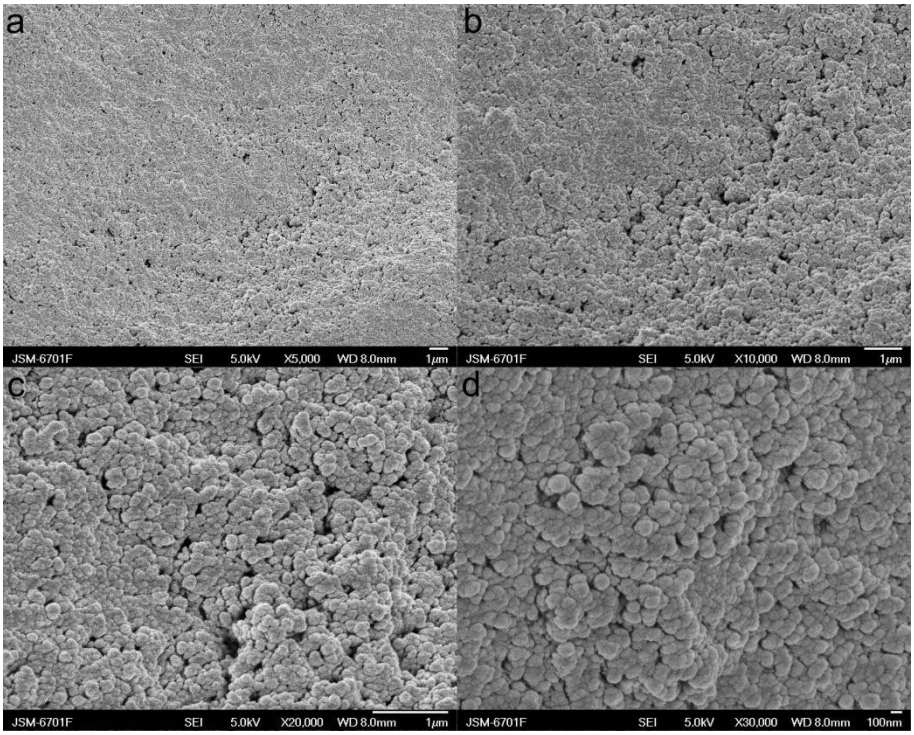

Figure 4. The SEM images of SiO_2@POS/N^+5 coating. SEM images of a) X5000, b) X10000, c) X20000 and d) X3000.

The SiO_2@POS/N^+5 particles are consisted of SiO_2 core and POS/N^+ shell, which can be proved by TEM images (Fig. 5). The good dispersity of these particles, as shown in Fig. 5a, is beneficial to construct micro/nano roughness for the resultant coatings. In Fig. 5b, the black opaque microscopic particles are SiO_2, which are coated by translucent material (POS/N^+). In addition, 21 particles were selected from Fig. S1, affording a maximum size of 14.92 nm, a minimum size of 7.08 nm, and an average size of 10.87 nm. It is shown that the SiO_2@POS/N^+5 particle of core-shell structure successfully prepared with good dispersity.

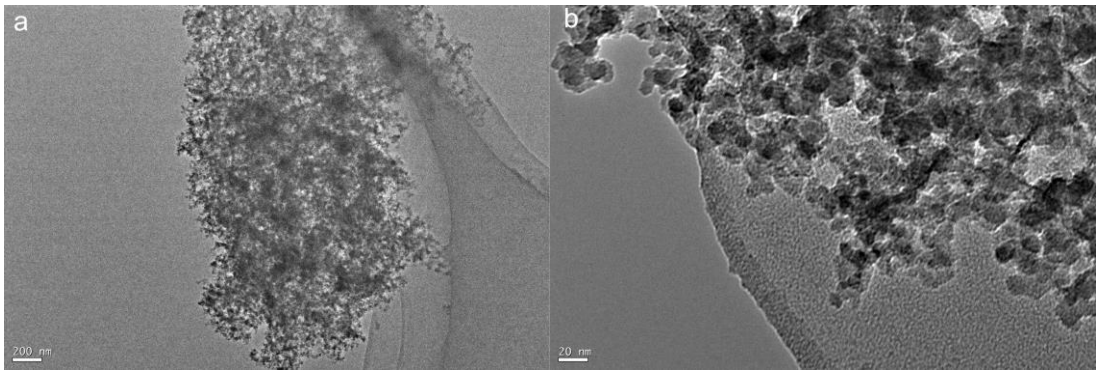

Figure 5. The TEM images of SiO_2@POS/N^+5.

Contact Angle and Mechanistic Measurements

The wettability of SiO_2@POS/N^+ coatings are depended on both micro/nano roughness and interface energy. The more micro/nano roughness and lower interface energy, the better enhanced superamphiphobic. The WCA and WSA for superhydrophobicity as well as the hexadecane OCA and hexadecane OSA for superoleophobicity were conducted for the measurement. As shown in Fig. 6, the

WCA and OCA of the different rate SiO_2@POS/N^+ in the resultant coatings are outstanding for almost all the samples, except the OCA for the sample 8 and 9, probably due to the incomplete hydrolysis polycondensation in a shorten reaction time. The more detailed WCA and OCA data can be seen in Table 1. The MPS, containing a polar functional group -SH, is a type of silane coupling agent, which would favourably promote hydrolytic polycondensation with TMFS and increase mechanical properties of SiO_2@POS/N^+ coating, but with the excess MPS hardly reducing interface energy further. Therefore, the WCA of the coating considerably decreased from 164.9 ± 1.9° to 146.5 ± 1.5° with the increase of MPS in samples 1 to 3 (Entries 1-3, Table 1). The best superhydrophobicity (WCA = 164.9 ± 1.9°, WSA = 4.0°) was achieved with the MPS concentration of 0.8 mM, accompanying poor superoleophobicity (OCA = 127.8 ± 1.4°). Notably, the additive amount of SiO_2 is crucial to the micro/nano roughness of SiO_2@POS/N^+ particles. A good superhydrophobicity (WCA = 160.8 ± 3.1°, WSA = 3.0°) together with good superoleophobicity (OCA = 152.5 ± 3.0°, OSA = 3.0°) were achieved with the additive amount of SiO_2 @ 0.12 g (Entry 5, Table 1). However, both the superhydrophobicity and superoleophobicity are decreased obviously as the reduction of reaction time (18 h, 12 h and 6 h), presumably due to decrease of the degree of hydrolysis and polycondensation (Entries 8-10, Table 1; Fig. 6, h-j). Thankfully, a simultaneously superhydrophobicity and superoleophobicity was achieved with the conditions in the sample 5 (Fig. 6e; Entry 5, Table 1). In addition, the peeling test by the tape 3M 810 revealed good mechanical properties of SiO_2@POS/N^+5 (Table.1). Ensured the coating surface and the adhesive surface of the tape contacted completely, the damage degree of coating surface is evaluated by the changes of its' WCA and OCA after quickly peeling off. The tests were terminated when the contact angle is lower than 150°. It is showed that the superhydrophobicity of the coating maintained for 350 times peel tests with 50 times for the superoleophobicity of the SiO_2@POS/N^+5 (Table.1) coating, demonstrating its' good mechanical properties.

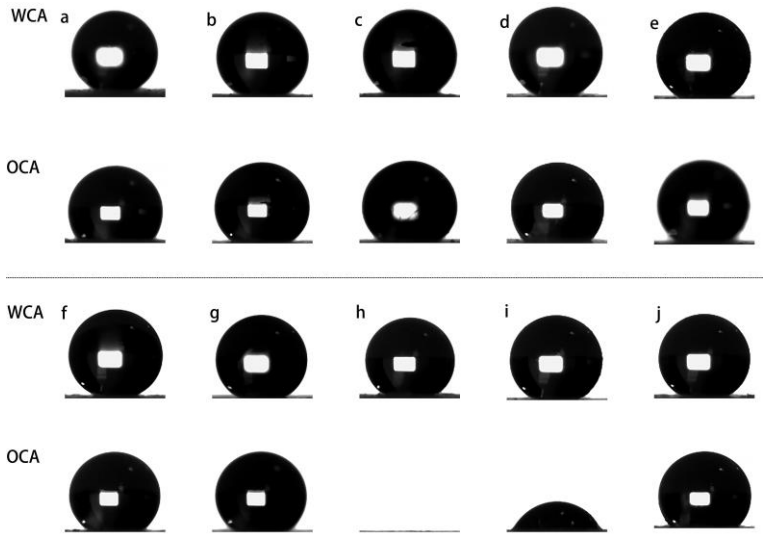

Figure 6. The WCA and OCA images of the different rate SiO_2@POS/N^+ coating samples 1-10.

Table. 1 The corresponding WCA and OCA data of the different rate SiO_2@POS/N^+ coating.

Samples	MPS (mM)	SiO_2 (g)	Time (h)	WCA (°)	WSA (°)	OCA (°)	OSA (°)
1	0.8	0.1	24	164.9 ± 1.9	4.0	127.8 ± 1.4	\
2	1.6	0.1	24	147.6 ± 1.6	5.0	141.0 ± 2.5	\
3	3.2	0.1	24	146.2 ± 1.5	4.0	136.4 ± 2.0	\
4	0.8	0.11	24	162.8 ± 3.1	5.0	141.2 ± 4.5	11

5	0.8	0.12	24	160.8 ± 3.1	3.0	152.5 ± 3.0	3.0
6	0.8	0.13	24	166.1 ± 1.5	2.0	147.8 ± 1.6	12
7	0.8	0.14	24	158.5 ± 0.2	4.0	150.2 ± 3.5	\
8	0.8	0.12	6	143.6 ± 1.9	\	0	\
9	0.8	0.12	12	148.3 ± 0.3	\	55.3 ± 9.3	\
10	0.8	0.12	18	149.9 ± 1.6	\	132.8 ± 6.9	\

Anticorrosion of the Coating

The anticorrosion performance of SiO_2@POS/N^+ coatings was disclosed by Tafel polarization curve as shown in Fig. 7 and Fig. S2 with the corresponding data listed in Table 2. Compared to the corrosion potential (E_{corr}) and corrosion current (I_{corr}) of the bare Q235SS of -873 mV and 1.119×10^{-5} A·cm^{-2} in 3.5 wt% NaCl, the E_{corr} and I_{corr} of the SiO_2@POS/N^+5 coating (Sample 5) are -463 mV and 1.926×10^{-9} mA·cm^{-2}, respectively. Therefore, the E_{corr} of SiO_2@POS/N^+5 coating is increased by 410 mV, while the I_{corr} of SiO_2@POS/N^+5 is decreased by nearly 4 orders of magnitude. The protection efficiency ($\eta = (I_a - I_b)/I_a$) defines the anticorrosion resistance, where I_a and I_b are corrosion current without coating and with coating, respectively. Thus, the η value of both SiO_2@POS/N^+5 and SiO_2@POS/N^+10 reach 99.9%, witnessing excellent corrosion resistance in 3.5 wt% NaCl. In addition, the larger the polarization resistance (R_p), the better the anticorrosion performance.[52] The R_p of each sample is shown in Table 2 with the R_p of sample 5 be the highest value of 8.851×10^6 Ω·cm^2, claiming the best anticorrosion performance. The corrosion rate (C_R) values were calculated by CHI660E in Table 2, where the M_{Fe} is the molecular weight of Q235SS, n is the number of electrons transferred in the corrosion reaction, and p is the density of the specimen (7.86 g cm^{-3}), it shows that the C_R of SiO_2@POS/N^+5 coating is the smallest.

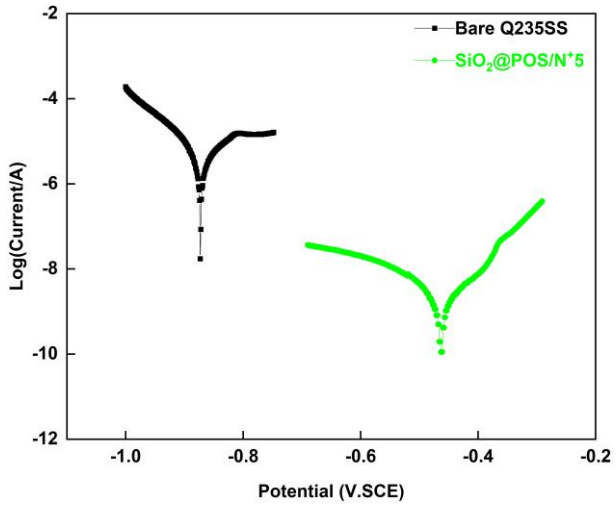

Figure 7. The Tafel polarization curves of bare Q235SS and SiO_2@POS/N^+5 coating.

Table. 2 The Tafel polarization curve values of the different rate SiO_2@POS/N^+ coatings. (Sample 1-10).

Samples	I_{corr} (A·cm^{-2})	E_{corr} (mV)	β_a (mV/decade)	β_c (mV/decade)	R_p (Ω·cm^2)	C_R (mil/year)	η (%)
Bare Q235SS	1.119×10^{-5}	-873	0.038	10.844	3.569×10^{3}	3.421×10^{0}	\
1	5.141×10^{-7}	-502	4.012	4.733	9.669×10^{4}	1.571×10^{-1}	95.40
2	1.652×10^{-6}	-569	4.076	4.123	3.209×10^{4}	5.049×10^{-1}	85.24
3	1.026×10^{-6}	-727	12.308	6.435	2.259×10^{4}	3.137×10^{-1}	90.83
4	3.983×10^{-7}	-558	4.968	4.555	1.146×10^{5}	1.217×10^{-1}	96.44
5	1.926×10^{-9}	-463	19.373	6.128	8.851×10^{6}	5.886×10^{-4}	99.98
6	5.206×10^{-8}	-482	4.077	5.435	8.779×10^{5}	1.519×10^{-2}	99.53
7	1.232×10^{-8}	-334	19.131	5.115	1.455×10^{6}	3.764×10^{-3}	99.88

8	5.667×10^{-7}	-399	11.013	3.417	5.316×10^{4}	1.732×10^{-1}	94.93
9	4.811×10^{-8}	-373	4.215	7.057	8.017×10^{5}	1.470×10^{-2}	99.57
10	5.855×10^{-9}	-373	2.958	6.891	7.538×10^{6}	1.789×10^{-3}	99.94

The anticorrosion performance of SiO_2@POS/N^+ coating was further revealed by EIS curve, the larger the impedance value, the better the corrosion resistance. The Nyquist plot of bare Q235SS shows in inset (Fig. 8a) with inset (1) for its equivalent electric circuit, in which R_s, CPE_{dl} and R_{ct} represent the solution resistance, the constant phase element of the double layer capacitor and the charge transfer resistor, respectively.[53] The fitting values of equivalent circuit corresponding to Q235SS present in Table S1, the fitting value of R_{ct} at only 474.6 Ω·cm^2 indicates that the bare Q235SS has very poor corrosion protection. Whilst the Nyquist plot of SiO_2@POS/N^+5 plugs in the same inset (Fig. 8a) with inset (2) for its equivalent electric circuit, where R_s, R_c, R_{ct} and C_{dl} represent solution resistance, superhydrophobic coating resistance, charge transfer resistance and double-layer capacitance, respectively.[54] In addition, the CPE_{cp} and R_{cp} are the capacitor and microporous resistor of 3M 75 adhensive layer, respectively. The fitting values of equivalent circuit corresponding to SiO_2@POS/N^+5 dramatically increased, affording R_{cp}, R_c and R_{ct} values of 9.353×10^6 Ω·cm^2, 2.008×10^7 Ω·cm^2 and 1.774×10^5 Ω·cm^2, respectively (Table S1). Compared to bare Q235SS, the resistance value of SiO_2@POS/N^+5 indicated a magnificent improvement for the super corrosion resistance of SiO_2@POS/N^+5. Meanwhile, the extremely high resistance values for all R_{cp}, R_c and R_{ct} together with the largest fitted value for R_c revealed a superamphiphobic layer on the surface with the outstanding corrosion protection. These results suggested that the internal 3M 75 adhesive layer not only enhances the mechanical properties of the coating, but also further improves its corrosion protection.

In addition, the time constant value of 1 for Q235SS in Fig. 8b indicates an extremely smooth microscopic surface of it after polishing, while the time constant value of SiO_2@POS/N^+5 coating is about 2, corresponding to 3M 75 adhesive layer and SiO_2@POS/N^+5 layer, respectively (Fig. 8b), the irregular vibrational peaks in the SiO_2@POS/N^+5 coating bode curve are probably due to the unevenness of the manual spraying. The impedance modulus of Q235SS is close to 0, indicating that Q235SS is easily corroded, whilst the impedance modulus of SiO_2@POS/N^+5 coating is close to 2.44×10^7, indicating an outstanding corrosion resistance performance of the obtained SiO_2@POS/N^+5 coatings (Fig. 8c).

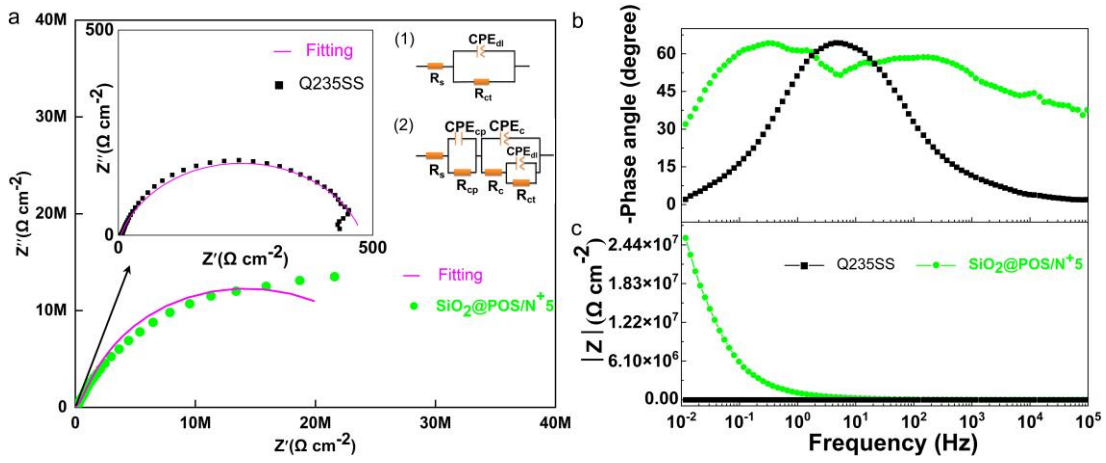

Figure 8. The Nyquist (a), bode (b) and impedance-modulus (c) plots of bare Q235SS and SiO_2@POS/N^+5 coating, respectively. The inset 1 and 2 (Fig. 8a) are equivalent electric circuits of bare Q235SS and SiO_2@POS/N^+5 coating, respectively.

The E_{ocp} variation (Fig. 9) and corrosion photographs (Fig. S3 and S4) of bare Q235SS and SiO_2@POS/N^+5 coating for long-term immersion in 3.5 wt% NaCl were conducted to prove the

anticorrosion durability of coatings. As shown in Fig. 9, the initial E_{ocp} of bare Q235SS was -0.517 V, the E_{ocp} rapidly dropped to -0.582 V in 3 h with an obvious color change in 2 h for the observation, indicating a slight corrosion phenomenon (Fig. S3). Thus, it demonstrated a rapid corrosion occurring to the bare Q235SS dipped in 3.5 wt% NaCl corrosion solution for continuous immersion of 2 h. Thereafter, the surface of the bare Q235SS was appeared local corrosion for 1 day of continuous immersion, the color of the corrosion solution turned from colorless-clear solution to a slight yellow cloudy solution with yellow corrosion products at the bottom of the beaker. After 2 days of continuous immersion, the surface of the steel piece was completely corrosive. In contrast, the initial E_{ocp} of SiO_2@POS/N^+5 coating was 0.008 V in the same environment, only a slightly increase with up to 0.02 V was obtained on average after 21 days of continuous immersion with a very clear and transparent corrosion solution (as good as the initial one, Fig. S4). Of particular note that the bubble layer on the surface of the SiO_2@POS/N^+5 coating was still present. The small sharp peak at the beginning of the E_{ocp} curve of SiO_2@POS/N^+5

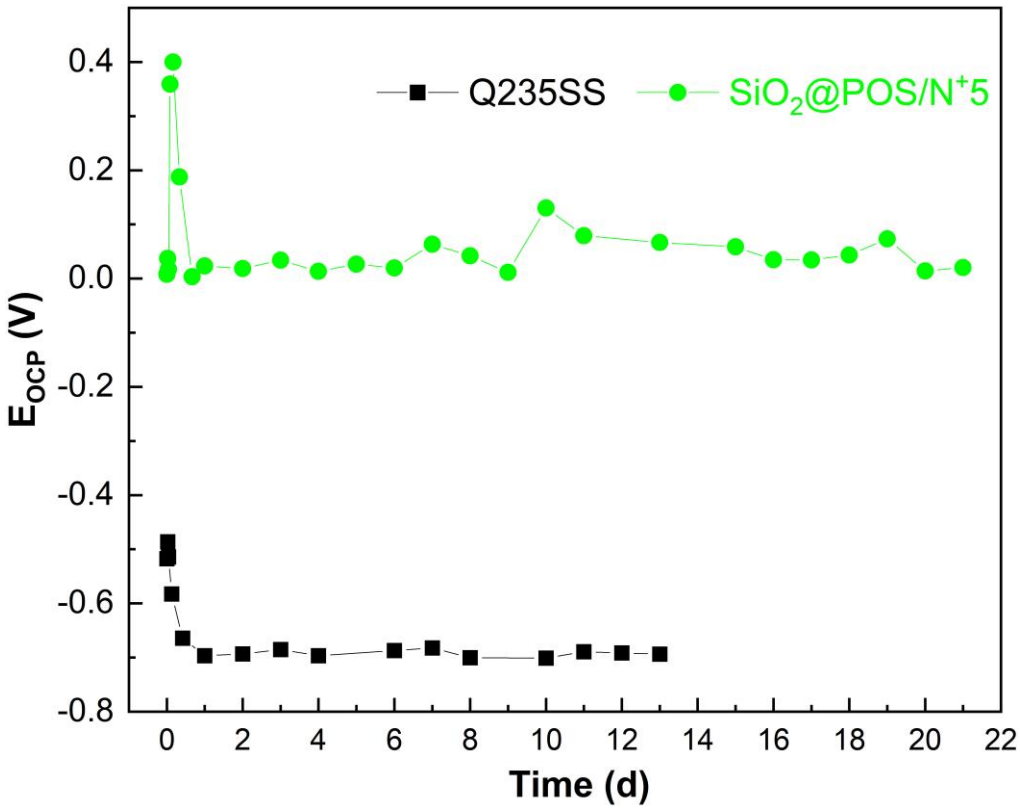

Figure 9. E_{ocp} variation of bare Q235SS and SiO_2@POS/N^+5 coatings with time by long-term immersion in 3.5 wt% NaCl solution.

coatings, presumably, due to the unestablished dynamic equilibrium of the microscopic system upon the immersion of coatings into the 3.5 wt% NaCl solution. The various of E_{ocp} tend to be stabilized when the microscopic dynamic system gradually settled down to the equilibrium. These results and observations indicated an outstanding and super durability against corrosion of the desired SiO_2@POS/N^+5 coatings.

Antibacterial Activity of the Coating

The antibacterial properties of SiO_2@POS/N^+5 were measured by the plate count method as shown in Fig. 10. Figure 10a and 10b are strains of *S. aureus* formed on LB agar plates, the blank group was

carried out in PBS buffer solution (Fig. 10a). Compared to the plate containing SiO_2@POS/N^+5 composite (Fig. 10b), there were no colonies observed on the plate, and the inhibitive rate of SiO_2@POS/N^+5 against *S. aureus* was calculated to be 100% (Table S2). Representative strains of *E. coli* formed on LB agar plates are shown in Figs. 10c and 10d. Compared with the control experiment (Fig. 10c), the number of colonies on the plate containing SiO_2@POS/N^+5 composite (Fig. 10d) changed significantly, the calculated inhibitive rate of SiO_2@POS/N^+5 against *E. coli* was 21% (Table S2). The results were obtained with the concentration of dispersed SiO_2@POS/N^+5 at 200 μg/mL, revealing its excellent antibacterial effect against *S. aureus*.[32, 33]

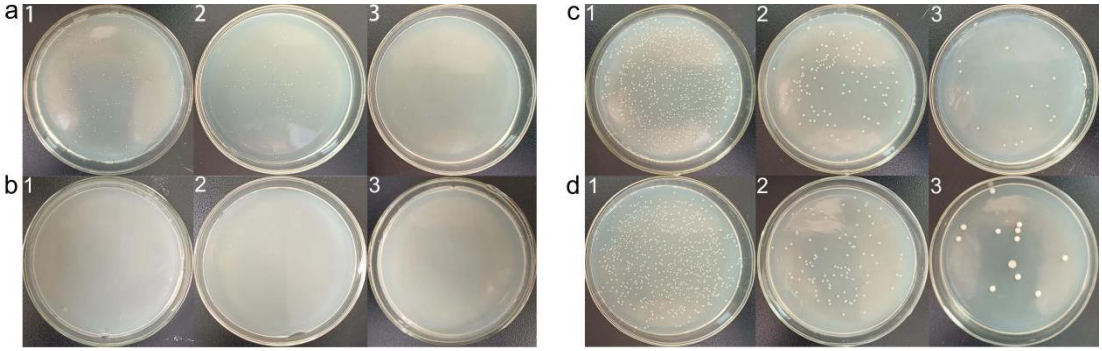

Figure 10. The colonies of *S. aureus* are formed on LB agar plates in the existence of PBS solution (10a) and SiO_2@POS/N^+5 (10b), respectively, a1~a3 and b1~b3 were serial 10^5, 10^6 and 10^7-fold dilutions. The colonies of *E. coli* are formed on LB agar plates in the existence of PBS solution (10c) and SiO_2@POS/N^+5 (10d), and c1~c3 and d1~d3 were serial 10^5, 10^6 and 10^7-fold dilutions.

4. Conclusion

In summary, a multifunctional coating with superamphiphobic, anticorrosion, and antibacterial properties was developed with designed functional groups, affording excellent performance for both anticorrosion and antibacterial activities. The SiO_2@POS/N^+5 composite material was synthesized through a simple one-pot sol-gel method, and the derived coatings was combined with 3M 75 adhesive spraying to enhance mechanical properties. The outstanding simultaneous superhydrophobicity (WCA = 160.8 ± 3.1°, WSA = 3.0°) and superoleophobicity (OCA = 152.5 ± 3.0°, OSA = 3.0°) of the composite were achieved with optimal conditions of the additive amounts of SiO_2, TMFS, MPS, CTAB, reaction time of 0.12 g, 15 mM, 0.8 mM, 0.4 mM, and 24 h, respectively. The Tafel and EIS curves are shown that the protection rate of SiO_2@POS/N^+5 coating was up to 99.98% together with outstanding and super durability against corrosion in 3.5 wt% NaCl solution for continuous long-term immersion (up to 21 days with almost consistent E_{ocp} on average as tested so far), possessing excellent mechanical properties. Whilst the SiO_2@POS/N^+5 composite material afforded almost full anti-bacterial effect against *S. aureus* as well. Therefore, this protocol demonstrates significant advantages for the development of desired superamphiphobic coatings with anticorrosion and antibacterial properties, providing simple and efficient applications in practice potentially.

Acknowledgement

The authors gratefully acknowledge the financial support by the Qinghai Normal University, Science and Technology Innovation Project (No. qhnuxskj2022019) and Middle Youth Research Fund Project (No. 1881030835).

Author Contributions:

Congcong Miao: Conceptualization, Methodology, Writing-original draft preparation. **Congcong Li**: Investigation, Methodology. **Xiaoxue Huang**: Investigation, Methodology. **Tiantian Yang**: Investigation, Data curation. **Yue Wang**: Validation, Data curation. **Junqiu Wang**: Investigation, Data curation. **Yanfang Wang**: Validation, Data curation. **Xiang Cui**: Visualization, Writing-original draft preparation. **Haidong Xu**: Conceptualization, Methodology, Supervision, Finding acquisition, Writing-original draft preparation. **Xiaofeng Wu**: Supervision, Visualization, Writing-Review & Editing

References

[1] S. T. Wang, K. S. Liu, X. Yao, L. Jiang, Bioinspired surface with superwettability: new insight on theory, design, and applications, Chem. Rev. 115, (**2015**), 8230-8293. Https://doi.org/10.1021/cr400083y.

[2] E. Vazirinasab, R. Jafari, G. Momen, Application of superhydrophobic coatings as a corrosion barrier: a review, Surf. Coat. Tech. 341, (**2018**), 40-56. https://doi.org/10.1016/j.surfcoat.2017.11.053.

[3] Y. Vasseghian, S. Hosseinzadeh, A. Khataee, E.N. Dragoi, The concentration of persistent organic pollutants in water resources: a global systematic review, meta-analysis and probabilistic risk assessment, Sci. Total Environ. 796, (**2021**), 149000. Https://doi.org/10.1016/j.scitotenv.2021.149000.

[4] J.A. Kumar, T. Krithiga, S. Sathish, A. Renita, D. Prabu, S. Lokesh, R. Geetha, S.K.R. Namasivayam, M. Sillanpaa, Sci. Total Environ. 831 (**2022**), 154808. Https://doi.org/10.1016/j.scitotenv.2022.154808.

[5] W.J. Wang, R.P. Liu, H.J. Chi, T. Zhang, Z.G. Xu, Y. Zhao, Durable superamphiphobic and photocatalytic fabrics: tackling the loss of super-non-wettability due to surface organic contamination, ACS Appl. Mater. Interfaces 11 (**2019**) 35327-35332. https://doi.org/10.1021/acsami.9b12141.

[6] T. Kamegawa, Y. Shimizu, H. Yamashita, Superhydrophobic surfaces with photocatalytic self-cleaning properties by nanocomposite coating of TiO_2 and polytetrafluoroethylene, Adv. Mater. 24 (**2012**) 3697-3700. https://doi.org/10.1002/adma.201201037.

[7] W.S.Y. Wong, T.P. Corrales, A. Naga, P. Baumli, A. Kaltbeitzel, M. Kappl, P. Papadopoulos, D. Vollmer, H.J. Butt, Microdroplet contaminants: when and why superamphiphobic surfaces are not self-cleaning, ACS nano, 14 (**2020**) 3836-3846. https://doi.org/10.1021/acsnano.9b08211.

[8] X.F. Ou, J.B. Cai, J.H. Tian, B.H. Luo, M.X. Liu, Superamphiphobic surfaces with self-cleaning and antifouling properties by functionalized chitin nanocrystals, ACS Sustain. Chem. Eng. 8 (**2020**) 6690-6699. https://doi.org/10.1021/acssuschemeng.0c00340.

[9] M. He, Q.L. Zhang, X.P. Zeng, D.P. Cui, J. Chen, H.L. Li, J.J. Wang, Y.L. Song, Hierarchical porous surface for efficiently controlling microdroplets' self-removal, Adv. Mater. 25 (**2013**) 2291-2295. https://doi.org/10.1002/adma.201204660.

[10] R.X. Yuan, S.Q. Wu, P. Yu, B.H. Wang, L.W. Mu, X.G. Zhang, Y.X. Zhu, B. Wang, H.Y. Wang, J.H. Zhu, Superamphiphobic and electroactive nanocomposite toward self-cleaning, antiwear, and anticorrosion coatings, ACS Appl. Mater. Interfaces 8 (**2016**) 12481-12493. https://doi.org/10.1021/acsami.6b03961.

[11] L.K. Gao, Z. Qiu, W.T. Gan, X.X. Zhan, J. Li, T.G. Qiang, Negative oxygen ions production by superamphiphobic and antibacterial TiO_2/Cu_2O composite film anchored on wooden substrates, Sci. Rep. 6 (**2016**) 1-10. https://doi.org/10.1038/srep26055.

[12] C.W. Peng, K.C. Chang, C.J. Weng, M.C. Lai, C.H. Hsu, S.C. Hsu, Y.Y. Hsu, W.I. Hung; Y. Wei, J.M. Yeh, Nano-casting technique to prepare polyaniline surface with biomimetic superhydrophobic structures for anticorrosion application, Electrochim. Acta 95 (**2013**) 192-199.

https://doi.org/10.1016/j.electacta.2013.02.016.

[13] Z.F. Tian, H.J. Yu, L. Wang, M. Saleem, F.J. Ren, P.F. Ren, Y.S. Chen, R.L. Sun, Y.B. Sun, L. Huang, Recent progress in the preparation of polyaniline nanostructures and their applications in anticorrosive coatings, RSC Adv. 4 (**2014**) 28195-28208. https://doi.org/10.1039/c4ra03146f.

[14] J.J. Conde, P. Ferreira-Aparicio, A.M. Chaparro, Anti-corrosion coating for metal surfaces based on superhydrophobic electrosprayed carbon layers, Appl. Mater. Today 13 (**2018**) 100-106. https://doi.org/10.1016/j.apmt.2018.08.001.

[15] H. Wang, J.H. Xu, X.S. Du, Z.L. Du, X. Cheng, H.B. Wang, A self-healing polyurethane-based composite coating with high strength and anti-corrosion properties for metal protection, Compos. Part B Eng. 225 (**2021**) 109273. https://doi.org/10.1016/j.compositesb.2021.109273.

[16] J.F. Wei, B.C. Li, L.Y. Jing, N. Tian, X. Zhao, J.P. Zhang, Efficient protection of Mg alloy enabled by combination of a conventional anti-corrosion coating and a superamphiphobic coating. Chem. Eng. J. 390 (**2020**) 124562. https://doi.org/10.1016/j.cej.2020.124562.

[17] L. Shen, Y. Li, W.J. Zhao, L.J. Miao, W.P. Xie, H.M. Lu, K. Wang, Corrosion protection of graphene-modified zinc-rich epoxy coatings in dilute NaCl solution. ACS Appl. Nano Mater. 2 (**2018**) 180-190. https://doi.org/10.1021/acsanm.8b01821.

[18] Y. Li, X.P. Lu, D. Mei, T. Zhang, F.H. Wang, Passivation of corrosion product layer on AM50 Mg by corrosion inhibitor, J. Magnes. Alloys (**2021**). https://doi.org/10.1016/j.jma.2021.11.020.

[19] X.W. Li, T. Shi, C. Liu, Q.X. Zhang, X.J. Huang, Multifunctional substrate of Al alloy based on general hierarchical micro/nanostructures: superamphiphobicity and enhanced corrosion resistance, Sci. Rep. 6 (**2016**) 1-11. https://doi.org/10.1038/srep35940.

[20] J.D. Gu, Microbiological deterioration and degradation of synthetic polymeric materials: recent research advances, Int. Biodeterior. Biodegrad. 52 (**2003**) 69-91. https://doi.org/10.1016/s0964-8305(02)00177-4.

[21] T.F. Mah, B. Pitts, B. Pellock, G.C. Walker, P.S. Stewart, G.A. O'Toole, A genetic basis for pseudomonas aeruginosa biofilm antibiotic resistance. Nature 426 (**2003**) 306-310. https://doi.org/10.1038/nature02122.

[22] G. O'Toole, H.B. Kaplan, R. Kolter, Biofilm formation as microbial development, Annu. Rev. Microbiol. 54 (**2000**) 49-79. https://doi.org/10.1146/annurev.micro.54.1.49.

[23] A. Algburi, N. Comito, D. Kashtanov, L.M.T. Dicks, M.L. Chikindas, Control of biofilm formation: antibiotics and beyond, Appl. Environ. Microb. 83 (**2017**). https://doi.org/10.1128/aem.02508-16.

[24] P.S. Stewart, J.W. Costerton, Antibiotic resistance of bacteria in biofilms, Lancet 358 (**2001**) 135-138. https://doi.org/10.1016/s0140-6736(01)05321-1.

[25] H.Q. Yang, Q. Zhang, Y.M. Li, G. Liu, Y. Huang, Effects of mechanical stress on protective properties of a marine coating on mild steel substrate, Corros. Sci. 177 (**2020**) 108986. https://doi.org/10.1016/j.corsci.2020.108986.

[26] R. Radha, D. Sreekanth, Electroless tin coated hydroxyapatite reinforced Mg-Sn alloy composite for enhanced bio corrosion resistance and bioactivity, Compos. Commun. 21 (**2020**) 100372. https://doi.org/10.1016/j.coco.2020.100372.

[27] H.P. Zheng,; Z. Li, L. Liu, F.D. Meng, Y. Cui, F.H. Wang, Superhydrophobic composite coatings in bacterial culture media: Durable antibacterial activity and enhanced corrosion resistance, Compos. Commun. 27 (**2021**) 100857. https://doi.org/10.1016/j.coco.2021.100857.

[28] S.F. Wen, P. Wang, L. Wang, Preparation and antifouling performance evaluation of fluorine-containing amphiphilic silica nanoparticles, Colloids Surf. A Physicochem. Eng. Aspects 611 (**2021**)

125823. https://doi.org/10.1016/j.colsurfa.2020.125823.

[29] H.Y. Chen, H.Z. Fan, N. Su, R.Y. Hong, X.S. Lu, Highly hydrophobic polyaniline nanoparticles for anti-corrosion epoxy coatings, Chem. Eng. J. 420 (**2021**) 130540. https://doi.org/10.1016/j.cej.2021.130540.

[30] H.D. Xu, C.C. Miao, L.Y. Wang, L.Zhang, H.X. Feng, J.H. Qiu, A robust superhydrophobic perfluoropolysiloxane and self-doped polyaniline/epoxy resin composite coating with excellent performance, Chem. Lett. 50 (**2021**) 1818. https://doi.org/10.1246/cl.210343.

[31] Y.J. Tuo, H.F. Zhang, L. Chen, W.P. Chen, X.W. Liu, K.G. Song, Fabrication of superamphiphobic surface with hierarchical structures on metal substrate, Colloids Surf. A Physicochem. Eng. Aspects 612 (**2021**) 125983. https://doi.org/10.1016/j.colsurfa.2020.125983.

[32] J.Z. Ma, C.Y. Liu, Y. Kai, CQDs-MoS_2 QDs loaded on dendritic fibrous nanosilica/hydrophobic waterborne polyurethane acrylate for antibacterial coatings, Chem. Eng. J. 429 (**2022**) 132170. https://doi.org/10.1016/j.cej.2021.132170.

[33] C.C. Miao, X.W. Xun, L.J. Dodd, S.Q. Niu, H.R. Wang, P.Y. Yan, X.C. Wang, J. Li, X.F. Wu, T. Hasell, Z.J Quan, Inverse vulcanization with SiO_2 embedded elemental sulfur for superhydrophobic, anti-corrosion, and antibacterial coatings, ACS Appl. Polym. Mater. 4 (**2022**) 4901-4911. https://doi.org/10.1021/acsapm.2c00490.

[34] F. Yang, W.Y.F. Zhou, F.H. Li, L. Yuan, Y.M. Diao, Y.L. Liu, Y. Pu, Y. Zhang, Y. Zhao, O. Jiang, D. Wang, Sprayable coating based on fluorinated silica nanocomposites with superhydrophobic and antibacterial properties for advanced concrete, Prog. Nat. Sci. Mater. Int. (**2022**). https://doi.org/10.1016/j.pnsc.2022.07.004.

[35] M. Tian, S. Cai, L. Ling, Y. Zuo, Z.Y. Wang , P.B. Liu, X.G. Bao, G.H. Xu, Superhydrophilic hydroxyapatite/hydroxypropyltrimethyl ammonium chloride chitosan composite coating for enhancing the antibacterial and corrosion resistance of magnesium alloy, Prog. Org. Coat. 165 (**2022**) 106745. https://doi.org/10.1016/j.porgcoat.2022.106745.

[36] S. Mumtaz, S. Ali, S. Mumtaz, T.A. Mughal, H.M. Tahir, H.A. Shakir, Chitosan conjugated silver nanoparticles: the versatile antibacterial agents, Polym. Bull. (**2022**) 1-18. https://doi.org/10.1007/s00289-022-04321-z.

[37] T. Suryaprabha, M.G. Sethuraman, Fabrication of copper-based superhydrophobic self-cleaning antibacterial coating over cotton fabric, Cellulose 24 (**2017**) 395-407. https://doi.org/10.1007/s10570-016-1110-z.

[38] H. Wen, S. Raza, P. Wang , Z.Y. Zhu, J.Y. Zhang, W. Huang, L.Z. Liang, H. Hu, L.B. Deng, C.K. Liu, Robust super hydrophobic cotton fabrics functionalized with Ag and PDMS for effective antibacterial activity and efficient oil-water separation, J. Environ. Chem. Eng. 9 (**2021**) 106083. https://doi.org/10.1016/j.jece.2021.106083.

[39] S.W. Park, D. Lee, Y.S. Choi, H.B. Jeon, C.H. Lee, J.H. Moon, I.K. Kwon, Mesoporous TiO_2 implants for loading high dosage of antibacterial agent, Appl. Surf. Sci. 303 (**2014**) 140-146. https://doi.org/10.1016/j.apsusc.2014.02.111.

[40] N.A.A. Yusof, N.M. Zain, N. Pauzi, Synthesis of ZnO nanoparticles with chitosan as stabilizing agent and their antibacterial properties against Gram-positive and Gram-negative bacteria, Int. J. Biol. Macromol. 124 (**2019**) 1132-1136. https://doi.org/10.1016/j.ijbiomac.2018.11.228.

[41] Y. Zhang, Y.F. Li, J.H. Li, Y.L. Gao, H. Tan, K.J. Wang, J.S. Li, Q. Fu, Synthesis and antibacterial characterization of waterborne polyurethanes with gemini quaternary ammonium salt, Sci. Bull. 60 (**2015**) 1114-1121. https://doi.org/10.1007/s11434-015-0811-2.

[42] Y. Bao, Y.X. Zhang, J.J. Guo, J.Z Ma, Y.Y. Lu, Application of green cationic silicon-based gemini surfactants to improve antifungal properties, fiber dispersion and dye absorption of sheepskin, J. Clean. Prod. 206 (**2019**) 430-437. https://doi.org/0.1016/j.jclepro.2018.09.186.

[43] C.Y. Dong, W.L. You, R.Q. Liuyang, Y.F. Lei, A.Q. Zhang, Y.L. Lin, Anti-Rhizoctonia solani activity by polymeric quaternary ammonium salt and its mechanism of action, React. Funct. Polym. 125 (**2018**) 1-10. https://doi.org/10.1016/j.reactfunctpolym.2018.01.020.

[44] J.Y. Li, Z.L. Sha, W.Y. Zhang, F.R. Tao, P.F. Yang, Preparation and antibacterial properties of gelatin grafted with an epoxy silicone quaternary ammonium salt, J. Biomater. Sci. Polym. Ed. 27 (**2016**) 1017-1028. https://doi.org/10.1080/09205063.2016.1175784.

[45] H.D. Xu, L. Zhang, L.Y. Wang, Y. Lu, H.X. Feng, A robust superhydrophobic/conductive composite coating with excellent anticorrosive performance, ChemistrySelect 6 (**2021**) 10412-10417. https://doi.org/10.1002/slct.202101043.

[46] J.X. Feng, H. Xu, S.H. Ye, G.F. Ouyang, Y.X. Tong, G.R. Li, Silica-polypyrrole hybrids as high-performance metal-free electrocatalysts for the hydrogen evolution reaction in neutral media, Angew. Chem. Int. Edit. 129 (**2017**) 8232-8236. https://doi.org/10.1002/anie.201702934.

[47] S. Pazokifard, S.M. Mirabedini, M. Esfandeh, S. Farrokhpay, Fluoroalkylsilane treatment of TiO_2 nanoparticles in difference pH values: Characterization and mechanism, Adv. Powder. Technol. 23 (**2012**) 428-436. https://doi.org/10.1016/j.apt.2012.02.006.

[48] Y.S.H Xu, M.H. Li, M.Y. Liu, Corrosion and fouling behaviors of phosphatized Q235 carbon steel coated with fluorinated polysiloxane coating, Prog. Org. Coat. 134 (**2019**) 177-188. https://doi.org/10.1016/j.porgcoat.2019.04.079.

[49] X.B. Chen, S.X. Zhou, B. You, L.M. Wu, Mechanical properties and thermal stability of ambient-cured thick polysiloxane coatings prepared by a sol-gel process of organoalkoxysilanes, Prog. Org. Coat. 74 (**2012**) 540-548. https://doi.org/10.1016/j.porgcoat.2012.01.021.

[50] C.A. Xu, Z.C. Qu, Z.Y. Tan, B.F. Nan, H.F. Meng, K. Wu, J. Shi, M.G. Lu, L.Y. Liang, High-temperature resistance and hydrophobic polysiloxane-based polyurethane films with cross-linked structure prepared by the sol-gel process, Polym. Test. 86 (**2020**) 106485. https://doi.org/10.1016/j.polymertesting.2020.106485.

[51] S. Sharifzadeh, S. Hassanajili, M.R. Rahimpour, Wettability alteration of gas condensate reservoir rocks to gas wetness by sol-gel process using fluoroalkylsilan, J. Appl. Polym. Sci. 128 (**2013**) 4077-4085. https://doi.org/10.1002/app.38632.

[52] P.P. Kong, H.X. Feng, N.L. Chen, Y. Lu, S.Y. Li, P. Wang. Polyaniline/chitosan as a corrosion inhibitor for mild steel in acidic medium. RSC Adv. 9(**2019**) 9211-9217. https://doi.org/10.1039/C9RA00029A.

[53] H.D. Xu, S.H. Fan, Y. Lu, H.X. Feng, J.H. Qiu. Proposal and verification of a novel superhydrophobic-conductive anti-corrosion polyaniline-silica coating. Bull. Chem. Soc. Jpn. 93 (**2020**) 1114-1120. https://doi.org/10.1246/bcsj.20200051.

[54] Y.Z. Cao, C. Chen, X. Lu, D. Xu, J. Huang, Z. Xin. Bio-based polybenzoxazine superhydrophobic coating with active corrosion resistance for carbon steel protection. Surf. Coat. Technol. 405 (**2021**) 126569. https://doi.org/10.1016/j.surfcoat.2020.126569.

Graphical Abstract

<Title>

A Robust Corrosive Coating Derived from Superhydrophobic, Superoleophobic, and Antibacterial SiO_2@POS/N^+ Composite Materials

<Authors' names>

Congcong Miao,[1] Congcong Li,[2] Xiaoxue Huang,[2] Tiantian Yang,[2] Yue Wang,[1] Junqiu Mao,[1] Yanfang Wang,[1] Xiang Cui,[1*] Haidong Xu[1*] and Xiaofeng Wu[3*]

<Summary>

A robust coating stemmed from superamphiphobic, anticorrosion and antibacterial SiO_2@POS/N^+ composite was prepared by sol-gel and spray method, with water contact angle and water sliding angle up to 160.8 ± 3.1 and 3.0° and oil contact angle and oil sliding angle up to 152.5 ± 3.0 and 3.0° were achieved, respectively. The SiO_2@POS/N^+5 coating has outstanding protection performance (Ƞ = 99.98%), mechanical properties, and corrosion durability (21 d) for continuous long-term immersion in 3.5 wt% NaCl solution test. Notably, the same composite material has almost full antibacterial effect against *S. aureus* as well.

<Diagram>